Spatiotemporal distribution, sources, and impact on atmospheric oxidation of reactive nitrogen oxides in the North China Plain agricultural regions in summer

Shaocong Wei[1], Qianqian Hong[2*], Wei Tan[3], Jian Chen[1], Tianhao Li[1], Xiaohan Wang[1], Jingkai Xue[4], Jiale Fang[1], Chao Liu[3], Aimon Tanvir[5], Chengzhi Xing[3], Cheng Liu[1, 3, 6, 7]

[1] Department of Precision Machinery and Precision Instrumentation, University of Science and Technology of China, Hefei 230026, China

[2] Key Laboratory of Ecosystem Carbon Source and Sink, China Meteorological Administration (ECSS-CMA), Wuxi University, Wuxi 214105, China

[3] Key Lab of Environmental Optics and Technology, Anhui Institute of Optics and Fine Mechanics, Hefei Institutes of Physical Science, Chinese Academy of Sciences, Hefei 230031, China

[4] School of Environmental Science and Optoelectronic Technology, University of Science and Technology of China, Hefei 230026, China

[5] College of Oceanography, Hohai University, Nanjing, 210024, China

[6] Center for Excellence in Regional Atmospheric Environment, Institute of Urban Environment, Chinese Academy of Sciences, Xiamen 361021, China

[7] Key Laboratory of Precision Scientific Instrumentation of Anhui Higher Education Institutes, University of Science and Technology of China, Hefei 230026, China

* Correspondence: hongqq@cwxu.edu.cn

Section S1. The Cloud effect.

Before conducting spectral analysis, it is essential to remove the impact of cloud effects. Wagner et al. proposed a method to determine cloud presence based on the color index (CI) [1]. CI refers to the ratio of solar radiation intensities at two different wavelengths:

$$CI = \frac{R_{320nm}}{R_{440nm}}$$

The CI_{meas} is calculated based on the detector signal as follows:

$$CI_{meas} = \frac{S_{320nm}}{S_{440nm}}$$

Here, S_λ represents the detector signal at wavelength λ.

Since the detector and grating efficiency depends on the wavelength, the observed CI_{meas} is not equal to CI. However, the CI and CI_{meas} are proportional:

$$CI = \beta \cdot CI_{meas}$$

Here, the β is a proportionality factor that depends on the efficiency of the spectrometer at different wavelengths.

Since Rayleigh scattering strongly depends on wavelength, CI is maximized under clear, cloudless conditions. In cloudy weather, the CI decreases, and cloud types can be determined by setting a CI threshold.

Section S2. The detailed introduction to the Ring effect and the I_0 effect

The Ring effect: The Ring effect is caused by the inelastic rotational Raman scattering of O_2 and N_2 in the atmosphere, which shortens the solar Fraunhofer lines [2]. Generally, the spectrum we measure is the sum of the elastic scattering process (Rayleigh scattering and Mie scattering) and the inelastic scattering process:

$$I = I_{elastic} + I_{inelastic} \quad (1)$$

However, formula (1) cannot completely remove the Fraunhofer structure from the observed spectrum, which may affect the retrieval of weak absorbing gases. Typically, the impact of the Ring effect can be mitigated by adding an absorption structure (the Ring effect absorption structure) during the spectral fitting process, as follows [3]:

$$-\ln(I_{meas}) = -\ln(I_{elastic} + I_{inelastic}) \quad (2)$$

Since $I_{elastic} \gg I_{inelastic}$, the formula can be expressed as:

$$-\ln(I_{elastic} + I_{inelastic}) \approx -\ln(I_{elastic}) + \frac{I_{inelastic}}{I_{elastic}} \quad (3)$$

Therefore, I_{Ring} can be calculated as follows:

$$I_{Ring} = \frac{I_{inelastic}}{I_{elastic}} \quad (4)$$

The I_0 effect: The I_0 effect arises due to the limited spectral resolution of MAX-DOAS instruments in the ultraviolet and visible bands, where solar and atmospheric absorption spectra are not fully resolvable [4,5]. To eliminate this effect, the absorption cross-sections of atmospheric trace gases can be corrected using a modified absorption cross-section.

First, the high-resolution solar spectrum $I_0(\lambda)$ is convolved with the instrument's slit function; then, the modeled absorption spectrum calculated from the highly resolved solar spectrum and absorption cross-section is convolved with the instrument's slit function; finally, assuming a

slant column density for an atmospheric trace gas. The corrected absorption cross-section can then be calculated as:

$$\sigma_{corrected}(\lambda, SCD) = \frac{-\ln\left(I^*(\lambda, SCD)\big/I_0^*(\lambda)\right)}{SCD}$$

In this study, the maximum SCD of the trace gas in the atmosphere is used to calculate the above absorption cross-section [5].

Section S3. WRF model Configurations.

The meteorological parameters (temperature and boundary layer height) in Wangdu were provided by WRF-Chem version 3.9.1. Comprehensive details about the WRF model are available on its official website (http://www.wrf-model.org/index.php). In this work, the simulation domain covered North China Plain and its surrounding area, with a center point of 38.0°N, 115.6°E. The simulation was configured with a horizontal resolution of 20 x 20 km, with 26 hybrid pressure-sigma levels vertically.

  The initial meteorological fields and boundary conditions were from the 6-h final operational global analysis (FNL) data. The data were provided by the National Centers for Environmental Prediction (NCEP), and it had a 1° × 1° spatial resolution. Furthermore, the NCEP Administrative Data Processing (ADP) Global Surface Observational Weather Data (ds461.0) and Upper Air Observational Weather Data (ds351.0) with 6-hourly temporal resolution were used to accurately reproduce the meteorology. The physical and chemical parameterization schemes adopted in this study are detailed in Table S1. Further configuration options of the model can be found in our previous study [6].

Table S1. Model configuration options.

Schemes	Description
Microphysics	Purdue Lin Scheme [7]
Longwave radiation	Rapid radiative transfer model (RRTMG) scheme [8]
Shortwave radiation	RRTMG scheme[8]
Cumulus parameterization	Grell–Freitas Ensemble Scheme [9]
Land surface	Unified Noah Land Surface Model [10]
Planetary boundary layer	Yonsei University scheme [11]

Table S2. The monthly average temperature and humidity during observation period.

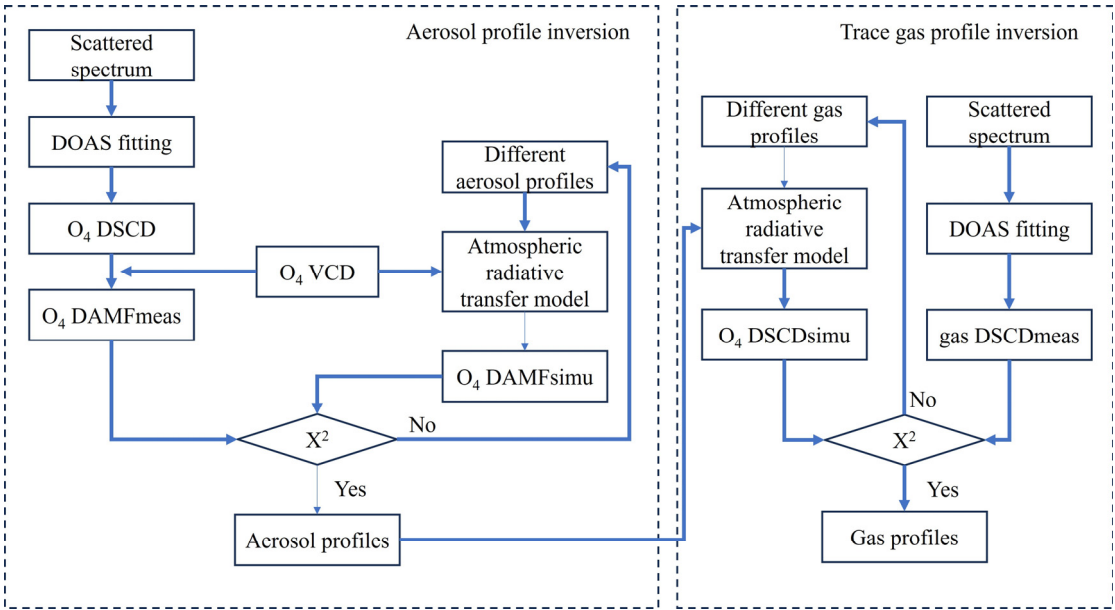| Month	Average temperature (℃)	Average relative humidity (%)
June	29.49	45.78
July	30.80	63.60
August	28.22	68.46

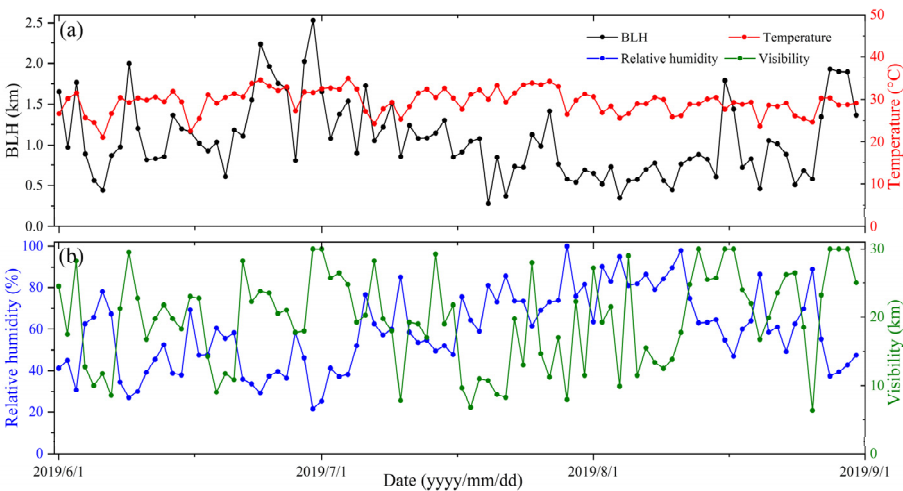**Figure S1.** Process of vertical profile retrievals.

Figure S2. The time series of meteorological information (boundary layer height, temperature, relative humidity, and visibility) in Wangdu area during observation period.
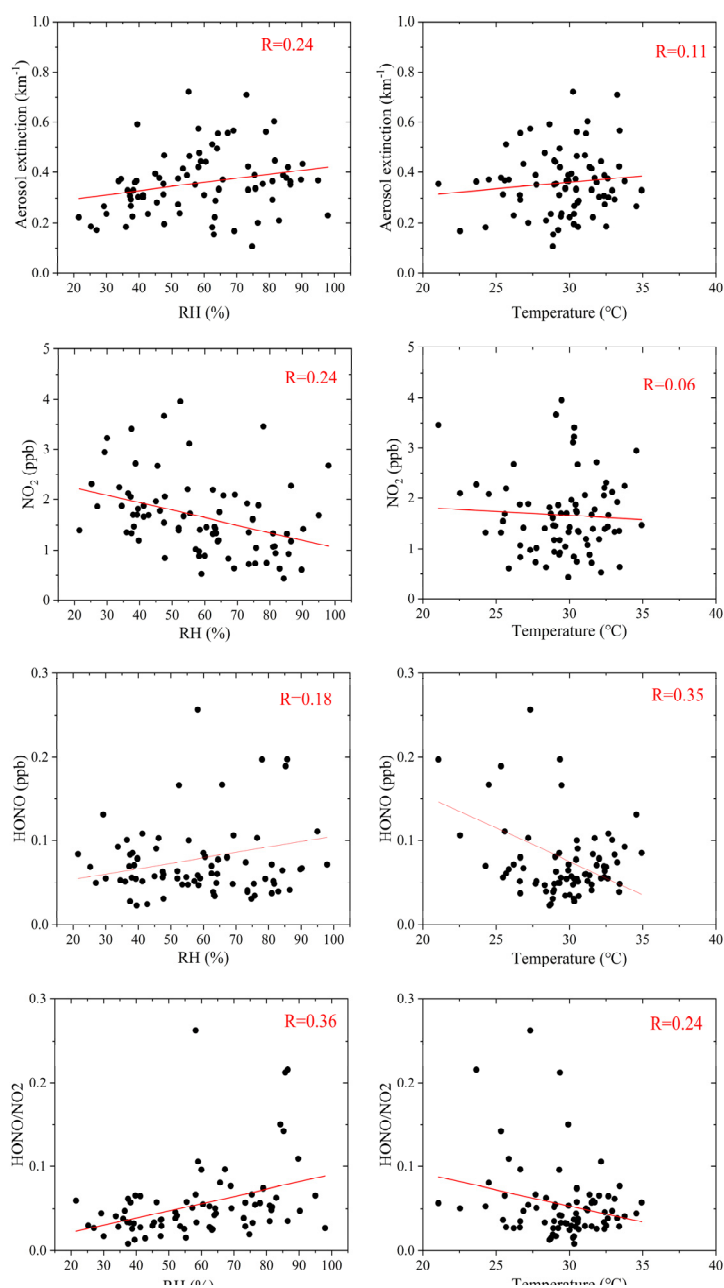
Figure S3. The scatter plots between meteorological information (RH and temperature) and pollutants (aerosols, NO₂, HONO, and NO₂/HONO).
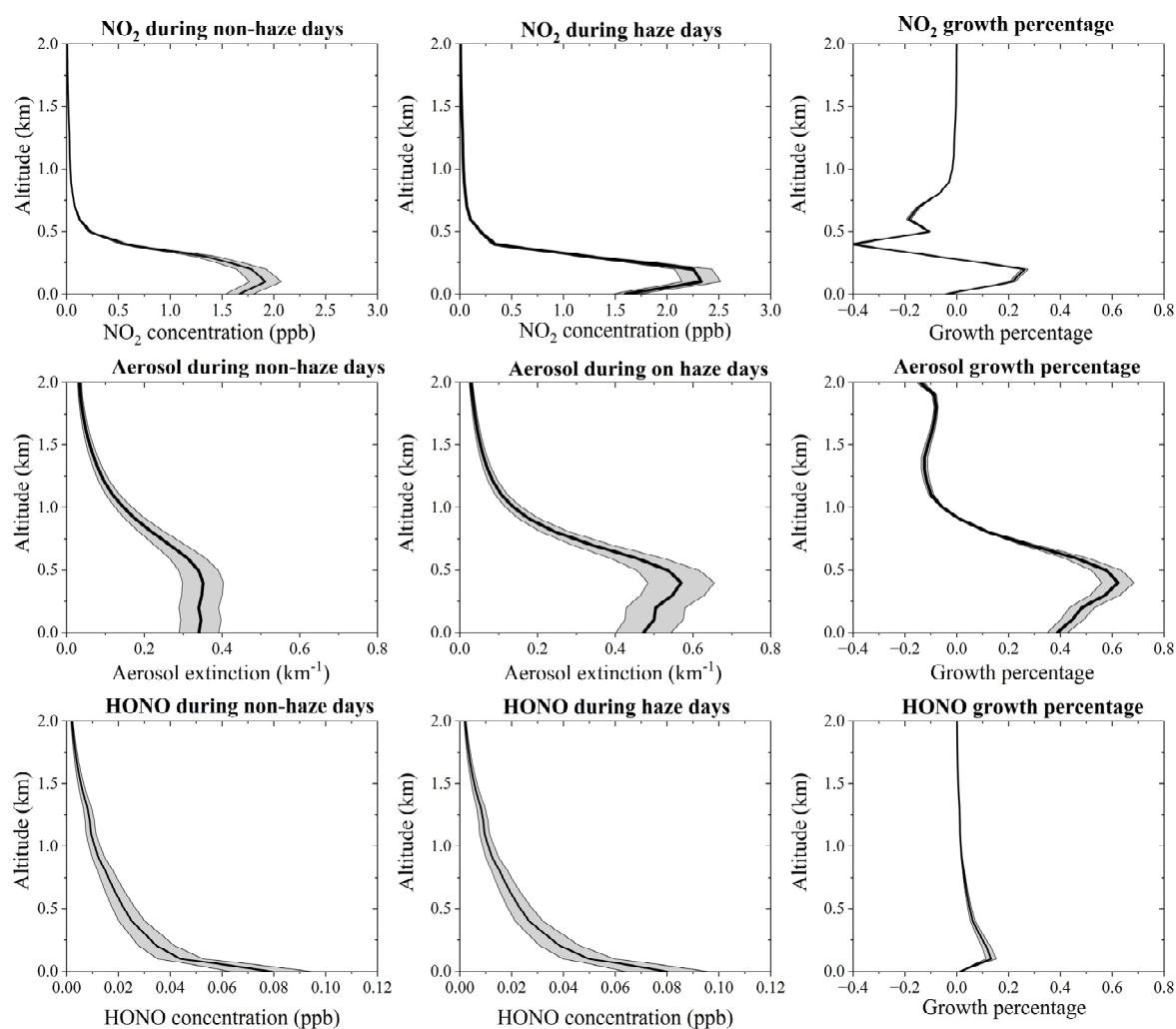
Figure S4. Mean profiles and error bars of aerosol extinction, NO_2, and HONO concentrations, and growth percentages during haze and non-haze days.
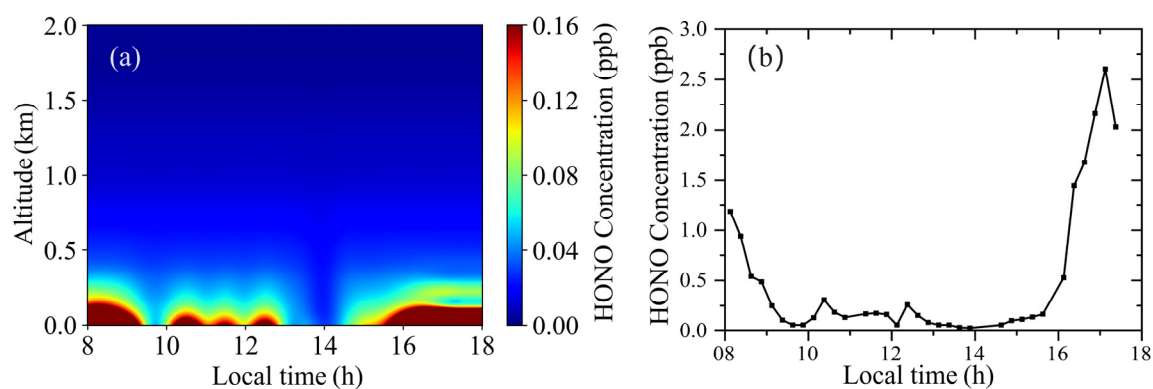
Figure S5. (a) Vertical diurnal variation of HONO on August 20th. (b) Diurnal variation of HONO within 0-100 meters altitude on August 20th.

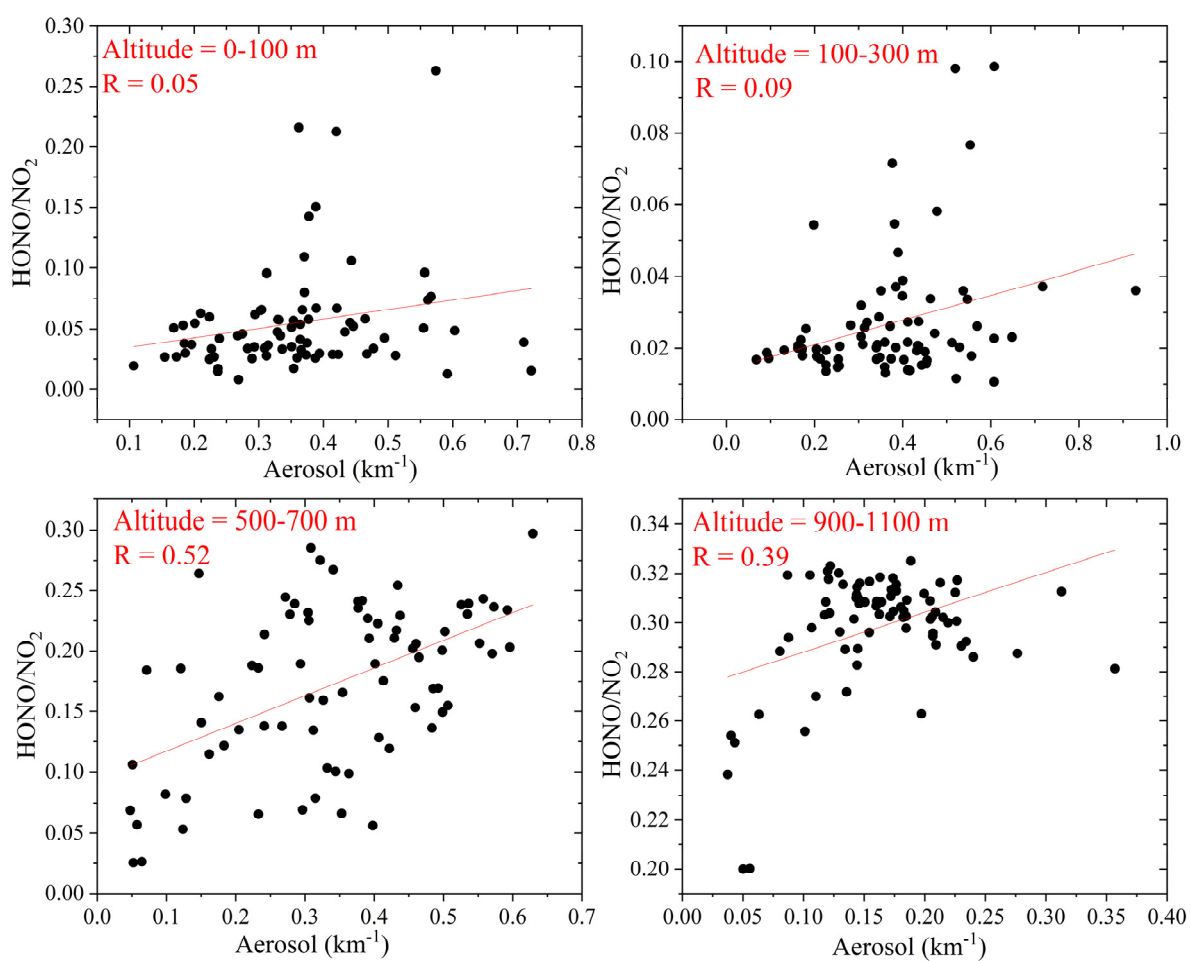**Figure S6.** Surrounding environment of the observation site.

Figure S7. The scatter plots between the ratio of HONO to NO₂ and aerosols at different altitudes.

References:

1. Wagner, T.; Apituley, A.; Beirle, S.; Dörner, S.; Friess, U.; Remmers, J.; Shaiganfar, R. Cloud Detection and Classification Based on MAX-DOAS Observations. *Atmos Meas Tech* **2014**, *7*, 1289–1320, doi:10.5194/amt-7-1289-2014.

2. GRAINGER, J.; RING, J. ANOMALOUS FRAUNHOFER LINE PROFILES. *NATURE* **1962**, *193*, 762-, doi:10.1038/193762a0.

3. Solomon, S.; Schmeltekopf, A.L.; Sanders, R.W. On the Interpretation of Zenith Sky Absorption Measurements. *J. Geophys. Res. Atmospheres* **1987**, *92*, 8311–8319, doi:10.1029/JD092iD07p08311.

4. Platt, U.; Marquard, L.; Wagner, T.; Perner, D. Corrections for Zenith Scattered Light DOAS. *Geophys. Res. Lett.* **1997**, *24*, 1759–1762, doi:10.1029/97GL01693.

5. Aliwell, S.R.; Van Roozendael, M.; Johnston, P.V.; Richter, A.; Wagner, T.; Arlander, D.W.; Burrows, J.P.; Fish, D.J.; Jones, R.L.; Tørnkvist, K.K.; et al. Analysis for BrO in Zenith-Sky Spectra: An Intercomparison Exercise for Analysis Improvement. *J. Geophys. Res. Atmospheres* **2002**, *107*, ACH 10-1, doi:10.1029/2001JD000329.

6. Liu, H.; Liu, C.; Xie, Z.; Li, Y.; Huang, X.; Wang, S.; Xu, J.; Xie, P. A Paradox for Air Pollution Controlling in China Revealed by "APEC Blue" and "Parade Blue." *Sci. Rep.* **2016**, *6*, 34408, doi:10.1038/srep34408.

7. CHEN, S.-H.; SUN, W.-Y. A One-Dimensional Time Dependent Cloud Model. *J. Meteor. Soc. Jpn. Ser II* **2002**, *80*, 99–118, doi:10.2151/jmsj.80.99.

8. Iacono, M.J.; Delamere, J.S.; Mlawer, E.J.; Shephard, M.W.; Clough, S.A.; Collins, W.D. Radiative Forcing by Long-Lived Greenhouse Gases: Calculations with the AER Radiative Transfer Models. *J. Geophys. Res. Atmospheres* **2008**, *113*, doi:10.1029/2008JD009944.

9. Grell, G.A.; Freitas, S.R. A Scale and Aerosol Aware Stochastic Convective Parameterization for Weather and Air Quality Modeling. *Atmos Chem Phys* **2014**, *14*, 5233–5250, doi:10.5194/acp-14-5233-2014.

10. Tewari, M. Implementation and Verification of the Unified Noah Land Surface Model in the WRF Model. **2004**.

11. Hong, S.-Y.; Noh, Y.; Dudhia, J. A New Vertical Diffusion Package with an Explicit Treatment of Entrainment Processes. *Mon. Weather Rev.* **2006**, *134*, 2318–2341, doi:10.1175/MWR3199.1.